

Redefining Orthogonal Co-Existence: A Mother Waveform Framework for DFT-Based Waveforms

Ayoub Ammar Boudjelal, Rania Yasmine Bir, and Hüseyin Arslan, *Fellow, IEEE*

Abstract—In this paper, we introduce the concept of a "mother waveform" to address key challenges in 5th generation (5G) and 6th generation (6G) networks, including spectrum efficiency, backward compatibility, enhanced flexibility, and the integration of joint sensing and communication (JSAC). We propose single-carrier interleaved frequency division multiplexing (SC-IFDM) as the mother waveform and demonstrate, through rigorous mathematical modeling, that it can generate all discrete Fourier transform (DFT)-based waveforms without requiring structural modifications. Specifically, by selectively configuring lattice indices and phase adjustments, SC-IFDM enables seamless adaptation to diverse waveforms, such as orthogonal frequency division multiplexing (OFDM), orthogonal chirp division multiplexing (OCDM), orthogonal time-frequency space (OTFS), affine frequency division multiplexing (AFDM), and frequency modulated continuous wave (FMCW) within a unified framework. Critical aspects such as coexistence strategies, and resource allocation are thoroughly explored. Simulation results demonstrate the proposed framework's ability to deliver superior communication performance, robust sensing capabilities, and efficient coexistence, surpassing traditional waveform designs in scalability and adaptability.

Index Terms—AFDM, OCDM, OFDM, OTFS, SC-IFDM.

I. INTRODUCTION

AS wireless communication progresses toward 6th generation (6G), the expectations for network capabilities and performance have significantly broadened [1]. Beyond achieving higher data rates, 6G aims to support a wide range of advanced applications [2], such as integrated artificial intelligence (AI) and communication, integrated sensing and communication (ISAC), and ubiquitous connectivity. Moreover, it seeks to enhance three existing scenarios: immersive communication, massive communication, and hyper-reliable low-latency communication. These scenarios are extensions of 5G's established use cases, including enhanced mobile broadband (eMBB), massive machine-type communications (mMTC), and ultra-reliable low latency communications (URLLC), as defined by IMT-2030 [3].

Addressing these diverse requirements demands a highly adaptable physical layer (PHY) capable of accommodating varying operational conditions, such as high-mobility environments, ultra-low latency, and the need for enhanced spectral efficiency (SE). However, developing such a flexible PHY

introduces considerable challenges, particularly in waveform design.

Orthogonal frequency division multiplexing (OFDM), a foundational waveform for 4th generation (4G) and 5th generation (5G) systems, has been widely adopted due to its SE, implementation simplicity, and compatibility with multiple-input multiple-output (MIMO) systems [4]. Despite these strengths, it has inherent drawbacks that become more pronounced as communication systems evolve. These include a high peak-to-average power ratio (PAPR), leading to power inefficiencies in uplink scenarios, particularly for energy-constrained devices, and poor performance in high-mobility environments, such as vehicle-to-everything (V2X) communication and high-speed railways [5], due to its sensitivity to Doppler shifts. Additionally, OFDM requires strict synchronization and suffers from large sidelobes, limiting its effectiveness in applications requiring joint sensing and communication (JSAC).

To address these limitations, several waveform modifications were introduced in 5G. One prominent example is discrete Fourier transform (DFT) spread OFDM (DFT-S-OFDM) [2], which has been widely adopted for uplink transmission in 5G due to its ability to reduce PAPR. DFT-S-OFDM retains the SE of OFDM while enhancing power efficiency, making it particularly well-suited for power-constrained devices. Additionally, variants such as zero-tail DFT-S-OFDM (ZT-DFT-S-OFDM) [6] and unique word DFT-S-OFDM (UW-DFT-S-OFDM) [7] were proposed to address out-of-band emissions and guard interval limitations, offering increased robustness against timing mismatches and multipath effects. While these advancements improved flexibility and performance, 5G waveforms still fail to meet the diverse requirements anticipated for 6G networks.

With the transition to 6G, the need for new waveforms capable of addressing high-mobility scenarios, doubly-dispersive channels, and ultra-low latency demands has become evident. Emerging candidates such as orthogonal time-frequency space (OTFS) [8], affine frequency division multiplexing (AFDM) [9], and orthogonal chirp division multiplexing (OCDM) [10] have been designed to overcome the limitations of 5G waveforms in specific use cases. For instance, OTFS operates in the delay-Doppler (DD) domain, offering exceptional resilience to Doppler effects, making it a strong candidate for high-mobility environments such as V2X and low Earth orbit (LEO) satellite communications [11]. On the other hand, AFDM demonstrates robustness in doubly-dispersive channels [12], where interference mitigation is critical. Similarly, OCDM, leveraging chirp signals, excels in combating inter-symbol interference (ISI),

The authors are with the Department of Electrical and Electronics Engineering, Istanbul Medipol University, Istanbul, 34810, Turkey (e-mail: ayoub.ammar@std.medipol.edu.tr; rania.bir@std.medipol.edu.tr; huseyinarslan@medipol.edu.tr).

making it highly suitable for scenarios demanding high SE under challenging channel conditions.

While each of these waveforms offers unique benefits, their coexistence within a single network introduces new challenges. 6G networks are expected to simultaneously support multiple waveforms, each tailored to specific applications with distinct performance requirements [13]. For instance, hyper reliable and low-latency communication demands ultra-low latency and high reliability, while massive communication emphasizes massive connectivity and energy efficiency [3]. This diversity necessitates a sophisticated framework capable of managing the orthogonal coexistence of these waveforms within shared time-frequency resources. Without effective coordination, waveform coexistence risks increased interference, suboptimal resource utilization, and degraded network performance.

The challenge extends beyond ensuring waveform compatibility to achieving high SE and low implementation complexity. For 6G networks to meet their potential, a unified waveform framework is required—one capable of dynamically generating multiple waveforms and ensuring their orthogonal coexistence within the same spectral resources. This framework would enable the network to adapt to the diverse needs of 6G applications, allowing different waveforms to operate seamlessly without mutual interference. Moreover, such a unified approach is critical not only for supporting the expansive range of 6G use cases but also for maintaining backward compatibility with existing 4G and 5G systems.

This paper addresses a critical challenge in 6G—the need for a unified waveform architecture that enables the seamless and orthogonal coexistence of diverse waveforms, particularly those based on DFT principles. We introduce the innovative concept of a “mother waveform,” a foundational waveform designed to generate multiple specialized waveforms tailored for different applications, ensuring minimal interference and optimal resource utilization. This mother waveform framework not only accommodates 6G waveforms such as OTFS, AFDM, and OCDM, but also maintains backward compatibility with legacy 5G waveforms like DFT-S-OFDM, offering a cost-effective and efficient solution for the seamless transition to 6G. The key contributions of this paper are as follows:

- This paper demonstrates that key waveforms used in 4G, 5G, and the emerging 6G networks, such as OFDM and single-carrier interleaved frequency division multiplexing (SC-IFDM), are all based on the DFT. We highlight how one of these DFT-based waveforms can serve as a “mother waveform,” capable of generating various other waveforms while maintaining efficiency and flexibility across generations.
- We propose an innovative framework that enables the derivation of multiple specialized “offspring” waveforms from the mother waveform. This framework offers enhanced flexibility in spreading techniques, resource allocation, and ensures backward compatibility, supporting seamless integration across different wireless standards.
- In addition, this paper introduces a novel flexible and sparse resource allocation scheme for OTFS in the time-

frequency (TF) domain, which allows a seamless coexistence scheme with other waveforms defined in the TF domain.

- Furthermore, novel orthogonal coexistence schemes that enable sweeping-frequency waveforms (e.g., frequency modulated continuous wave (FMCW) [14], [15]) and constant-frequency waveforms (e.g., SC-IFDM [16], [17], OTFS) are proposed to operate simultaneously with minimal interference. This ensures efficient and interference-free communication within the same network, crucial for complex multi-waveform 6G environments.
- We conduct an in-depth, simulation-based analysis to assess the proposed coexistence schemes, focusing on key performance metrics such as complexity, bit error rate (BER), system capacity, and sensing capabilities. These evaluations demonstrate the effectiveness of our approach across diverse network scenarios and applications.

The remainder of this article is organized as follows. Section II presents preliminaries about the existing waveforms in the literature. Section III establishes the connection between SC-IFDM signal to different DFT waveforms. Section IV presents novel practical co-existence cases. In Section V, the simulation results are provided and finally, Section VI concludes the paper.

Notation: Bold uppercase \mathbf{A} , bold lowercase \mathbf{a} , and unbold letters A , a denote matrices, column vectors, and scalar values, respectively. $(\cdot)^{-1}$ denote the inverse operators. $\delta(\cdot)$ denotes the Dirac-delta function. $\mathbb{C}^{M \times N}$ denotes the space of $M \times N$ complex-valued matrices.

II. PRELIMINARIES

In this section, we introduce the discrete Zak transform (DZT), followed by a discussion on key waveform models such as OFDM, SC-IFDM, OTFS, FMCW, OCDM, and AFDM.

A. Discrete Zak Transform

The DD domain, also known as Zak space, is an intermediate space between the direct signal space “time” and the Fourier space “frequency”. Assume the DD grid is discretized into M delays and N Doppler bins, and consider an arbitrary discrete MN -point sequence \mathbf{s} . The DZT of \mathbf{s} is an isometry $\mathbb{C}^{MN} \rightarrow \mathbb{C}^{N \times M}$ expressed as [18]

$$X(k, l) = \frac{1}{\sqrt{N}} \sum_{n=0}^{N-1} s(l + nM) e^{-j2\pi \frac{k}{N} n}, \quad (1)$$

for $0 \leq l < M, 0 \leq k < N$.

To compute $X(k, l)$, M DFT blocks of size N are required for the data sets $s(l), s(l+M), \dots, s(l+(N-1)M)$, $0 \leq l < M$. The original sequence \mathbf{s} can be recovered from its DZT using the inverse discrete Zak transform (IDZT), as follows

$$s(l + nM) = \frac{1}{\sqrt{N}} \sum_{k=0}^{N-1} X(k, l) e^{j2\pi \frac{k}{N} n} \quad (2)$$

for $0 \leq l < M, 0 \leq n < N$.

The vectorized output of the IDZT for a matrix \mathbf{X} can be written as

$$\mathbf{s} = (\mathbf{F}_N^H \otimes \mathbf{I}_M) \text{vec}(\mathbf{X}), \quad (3)$$

where \mathbf{F}_N is $N \times N$ unitary DFT matrix and \mathbf{I}_M is the $M \times M$ identity matrix.

B. OFDM Signal Model

Consider a wireless communication system where N data symbols are modulated using OFDM over a total bandwidth B , operating at the carrier frequency f_c . The OFDM modulator distributes the symbols $\{X(k), k = 0, \dots, N-1\}$ in the frequency domain. Denoting the bandwidth of each of the N subcarriers as $\Delta f = B/N$, the time duration of one OFDM symbol is $T = 1/\Delta f$. The frequency samples $X(k)$ are then converted to the time domain using an inverse discrete Fourier transform (IDFT) operation. The discrete output of an OFDM modulator is

$$s^{\text{OFDM}}(l) = \frac{1}{\sqrt{N}} \sum_{k=0}^{N-1} x^{\text{OFDM}}(k) e^{j2\pi \frac{kl}{N}}, \quad (4)$$

or equivalently in matrix form is given as

$$\mathbf{s}^{\text{OFDM}} = \mathbf{F}_N^H \mathbf{x}^{\text{OFDM}}. \quad (5)$$

C. SC-IFDM Signal Model

In SC-IFDM, $M \times N$ data symbols are modulated by mapping them to N DFT blocks, each of size M . The outputs of these blocks are interleaved before applying a final MN -point IDFT. The resulting time-domain signal $s^{\text{SC-IFDM}}(p)$, with the data symbols $X^{\text{SC-IFDM}}(k, l)$ for $k = 0, \dots, N-1$ and $l = 0, \dots, M-1$, is given for $p = 0, 1, \dots, MN-1$ as [19]

$$s^{\text{SC-IFDM}}(p) = \frac{1}{\sqrt{N}} \sum_{k=0}^{N-1} X^{\text{SC-IFDM}}(k, [p]_M) e^{j2\pi \frac{kp}{MN}}. \quad (6)$$

By setting $p = l + nM$ with $n = 0, \dots, N-1$, we get

$$s^{\text{SC-IFDM}}(l + nM) = \frac{1}{\sqrt{N}} \sum_{k=0}^{N-1} X^{\text{SC-IFDM}}(k, l) e^{j2\pi \frac{k(l+nM)}{MN}}. \quad (7)$$

To express the discrete time-domain SC-IFDM baseband signal in (7) in a matrix-vector form, we write the output of the M -point DFT block after interleaving as

$$s(k + mN) = \frac{1}{\sqrt{M}} \sum_{l=0}^{M-1} X^{\text{SC-IFDM}}(k, l) e^{-j2\pi \frac{l}{M} m}, \quad (8)$$

which is then written in matrix form as

$$\mathbf{s} = \mathbf{\Gamma} (\mathbf{I}_N \otimes \mathbf{F}_M) \mathbf{x}^{\text{SC-IFDM}}, \quad (9)$$

where $\mathbf{x}^{\text{SC-IFDM}} = \text{vec}(\mathbf{X}^{\text{SC-IFDM}})$, $\mathbf{\Gamma} = [\mathbf{\Gamma}_0, \dots, \mathbf{\Gamma}_{M-1}]^T$ is the interleaving matrix, where each $\mathbf{\Gamma}_m$ is defined as $\text{CircShift}((\mathbf{I}_N \otimes \mathbf{\Upsilon}), m)$ for $m = 0, \dots, M-1$ and $\mathbf{\Upsilon} = [1, \mathbf{0}_{M-1}]$. Thus, (7) is reformulated as

$$\mathbf{s}^{\text{SC-IFDM}} = \mathbf{F}_{MN}^H \mathbf{\Gamma} (\mathbf{I}_N \otimes \mathbf{F}_M) \mathbf{s}^{\text{SC-IFDM}}. \quad (10)$$

D. OTFS Signal Model

In OTFS, $M \times N$ data symbols are modulated over a total bandwidth B at the carrier frequency f_c . The OTFS modulator maps the data symbols $\{X^{\text{OTFS}}(k, l), k = 0, \dots, N-1, l = 0, \dots, M-1\}$ onto the DD grid. Each subcarrier occupies a bandwidth of $\Delta f = B/M$, resulting in a time duration of $T = 1/\Delta f$. Consequently, an OTFS frame spans a total duration of NT . The mapped symbols are transformed into the TF domain using the inverse symplectic finite Fourier transform (ISFFT), which is defined as

$$X^{\text{TF}}(n, m) = \frac{1}{\sqrt{MN}} \sum_{l=0}^{M-1} \sum_{k=0}^{N-1} X^{\text{OTFS}}(k, l) e^{j2\pi (\frac{nk}{N} - \frac{ml}{M})}. \quad (11)$$

The time-domain OTFS signal is then produced by converting the TF samples to the time domain using the IDFT, i.e.,

$$s^{\text{OTFS}}(m + nM) = \frac{1}{\sqrt{M}} \sum_{m=0}^{M-1} X^{\text{TF}}(n, m) e^{j2\pi \frac{m}{M} n}. \quad (12)$$

Note that the total length of the discrete sequences representing the frame is $M \times N$. Substituting (11) in (12) and using $(1/M) \sum_{m=0}^{M-1} e^{j2\pi m(l-l')/M} = \delta(l-l')$, we obtain

$$s^{\text{OTFS}}(l + nM) = \frac{1}{\sqrt{N}} \sum_{k=0}^{N-1} X^{\text{OTFS}}(k, l) e^{j2\pi \frac{k}{N} n}, \quad (13)$$

which is precisely the IDZT described in (2). As a result, the DFT-based cascaded ISFFT and OFDM modulation have a similar structure to the IDZT. In order to obtain the discrete sequence without employing the ISFFT, one can use the IDZT. Similar outcomes can be attained for the receiver when the DFT-based OFDM demodulation is coupled with the symplectic finite Fourier transform (SFFT), which yields the DZT, i.e.,

$$\mathbf{s}^{\text{OTFS}} = (\mathbf{F}_N^H \otimes \mathbf{I}_M) \text{vec}(\mathbf{X}^{\text{OTFS}}) = (\mathbf{F}_N^H \otimes \mathbf{I}_M) \mathbf{x}^{\text{OTFS}}. \quad (14)$$

E. FMCW Signal Model

Consider a linear FMCW signal, $s^{\text{FMCW}}(t)$, sweeps linearly over a bandwidth B_c within a time duration T_c . It is written in time-domain as [20]

$$s^{\text{FMCW}}(t) = e^{j\pi\eta t^2}, \quad 0 \leq t < T_c, \quad (15)$$

where $\eta = \frac{B_c}{T_c}$ is the chirp rate, and $\eta, T_c, B_c \in \mathbb{R}$. For a time-bandwidth product $MN = \eta T_c^2$ that is a positive integer, the FMCW signal can be critically sampled at intervals $t = \frac{p}{MN} T_c$, leading to the discrete form given below

$$s^{\text{FMCW}}(p) = e^{j\pi \frac{p^2}{MN}}, \quad 0 \leq p < MN. \quad (16)$$

F. OCDM Signal Model

In OCDM, a set of $M \times N$ orthogonal chirps are used to modulate $M \times N$ data symbols x using the inverse discrete Fresnel transform (IDFnT). The discrete-time baseband OCDM signal is expressed as [21]

$$s^{\text{OCDM}}(p) = \frac{e^{j\frac{\pi}{4}}}{\sqrt{MN}} \sum_{i=0}^{MN-1} x^{\text{OCDM}}(i) e^{-j\pi \frac{(p-i)^2}{MN}}, \quad (17)$$

which can equivalently be expressed in matrix-vector form as

$$\mathbf{s}^{\text{OCDM}} = \mathbf{\Phi}^H \mathbf{x}^{\text{OCDM}}, \quad (18)$$

where $\mathbf{\Phi}$ is the unitary discrete Fresnel transform (DFnT) matrix, defined with the $(p, i)^{\text{th}}$ elements as

$$\Phi(p, i) = \frac{e^{j\frac{\pi}{4}}}{\sqrt{MN}} e^{-j\pi \frac{(p-i)^2}{MN}}, [MN]_2 = 0. \quad (19)$$

The matrix $\mathbf{\Phi}$ can be decomposed into a DFT matrix with additional quadratic phase shifts

$$\mathbf{\Phi} = \mathbf{\Theta}_1 \mathbf{F} \mathbf{\Theta}_2, \quad (20)$$

where $\mathbf{\Theta}_1$ and $\mathbf{\Theta}_2$ are diagonal phase matrices given by $\mathbf{\Theta}_1(p, p) = e^{-j\frac{\pi}{4}} e^{j2\pi \frac{p^2}{MN}}$ and $\mathbf{\Theta}_2(i, i) = e^{j2\pi \frac{p^2}{MN}}$.

G. AFDM Signal Model

In AFDM, a vector of symbols $\mathbf{x}^{\text{AFDM}} \in \mathbb{C}^{MN \times 1}$ is mapped into the twisted TF chirp domain using the inverse discrete affine Fourier transform (IDAFT), described by [9]

$$s^{\text{AFDM}}(p) = \frac{1}{\sqrt{MN}} \sum_{i=0}^{MN-1} x^{\text{AFDM}}(i) e^{j2\pi(c_1 p^2 + c_2 i^2 + pi/MN)}, \quad (21)$$

where the i -th unmodulated element of the TF chirp domain is given by

$$s^{\text{AFDM},i}(p) = e^{j2\pi(c_1 p^2 + c_2 i^2 + pi/MN)}. \quad (22)$$

In a matrix form, (21) is represented as

$$\mathbf{s}^{\text{AFDM}} = \mathbf{\Lambda}_{c_1}^H \mathbf{F}^H \mathbf{\Lambda}_{c_2}^H \mathbf{x}^{\text{AFDM}}, \quad (23)$$

where $\mathbf{\Lambda}_{c_1}^H \mathbf{F}^H \mathbf{\Lambda}_{c_2}^H \in \mathbb{C}^{MN \times MN}$ represents the forward MN -point discrete affine Fourier transform (DAFT) matrix, and the diagonal chirp matrix with a central digital frequency of c_i represented by $\mathbf{\Lambda}_{c_i} \triangleq \text{diag}[e^{-j2\pi c_i(0)^2}, \dots, e^{-j2\pi c_i(MN-1)^2}]$. This structure shows that AFDM can also be classified as a DFT-based waveform due to its use of chirp modulation.

III. SC-IFDM TO DIFFERENT DFT WAVEFORMS

In this section, we demonstrate that all discussed waveforms (OFDM, OTFS, FMCW, OCDM, AFDM) can be efficiently generated using the general structure of SC-IFDM.

A. SC-IFDM to OFDM

When SC-IFDM is reduced to a single-dimensional waveform by setting $M = 1$ in (7), the result is the following expression

$$s_{\text{SC-IFDM}}^{\text{OFDM}}(l) = \frac{1}{\sqrt{N}} \sum_{k=0}^{N-1} x^{\text{OFDM}}(k) e^{j2\pi \frac{k}{N} l}, \quad (24)$$

which exactly matches the OFDM signal, as described in (4).

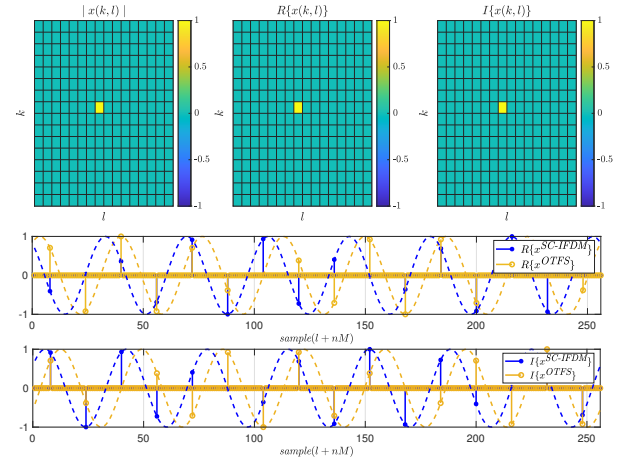


Fig. 1. SC-IFDM to OTFS, $M = 16$, $N = 16$.

B. SC-IFDM to OTFS

By analyzing (7), it becomes clear that SC-IFDM and OTFS exhibit similar data-spreading behavior, with the primary difference being the phase shifts applied in the time and the DD domains. In OTFS modulation, each delay bin contains M repetitions of the Doppler domain data. This repetition can be achieved by performing an N -point IDFT followed by upsampling the output by M samples, which is equivalent to taking an MN -point IDFT. The OTFS time domain signal in (13) can be represented in terms of SC-IFDM as

$$\begin{aligned} X_{\text{SC-IFDM}}^{\text{OTFS}}(k, l) &= \frac{1}{\sqrt{N}} \sum_{n=0}^{N-1} s^{\text{OTFS}}(l + nM) e^{-j2\pi \frac{k(l+nM)}{MN}} \\ &= X^{\text{OTFS}}(k, l) \omega_k^l, \end{aligned} \quad (25)$$

where $\omega_k^l = e^{j2\pi(\frac{-kl}{MN})}$. Hence, the difference between OTFS and SC-IFDM is merely a phase shift, as illustrated in Fig. 1. Both waveforms share similar structures, and OTFS can be generated from SC-IFDM by applying phase-adjustments to the same data. The matrix form of (25) is written as

$$\mathbf{s}_{\text{SC-IFDM}}^{\text{OTFS}} = \mathbf{F}_{MN}^H \mathbf{\Gamma} (\mathbf{I}_N \otimes \mathbf{F}_M) \mathbf{\Psi} \mathbf{x}^{\text{OTFS}}, \quad (26)$$

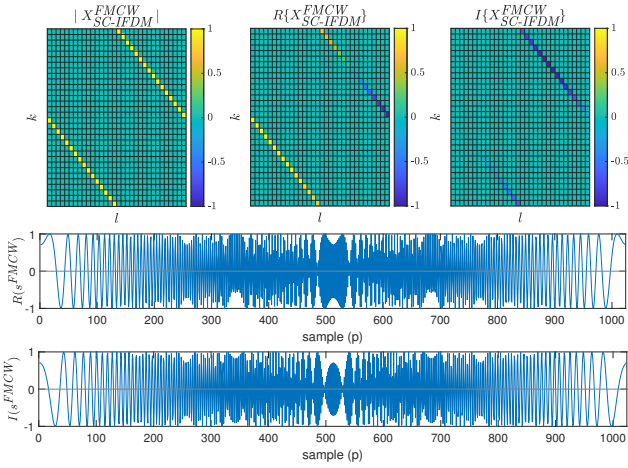
where $\mathbf{\Psi} = \text{diag}\{\omega_0, \dots, \omega_{N-1}\}$ and $\omega_k = [\omega_k^0, \dots, \omega_k^{M-1}]^T$, with $\omega_k^l = e^{-j2\pi \frac{kl}{MN}}$. This allows SC-IFDM to experience the same delay and Doppler shifts as OTFS under doubly dispersive channels, and their behavior in the effective channel is equivalent. The received SC-IFDM signal, $\mathbf{y}^{\text{SC-IFDM}}$, can be written as

$$\mathbf{y}^{\text{SC-IFDM}} = \mathbf{H} \mathbf{F}_{MN}^H \mathbf{\Gamma} (\mathbf{I}_N \otimes \mathbf{F}_M) \mathbf{x}^{\text{SC-IFDM}} + \mathbf{w}, \quad (27)$$

where \mathbf{H} represents the R -tap time-domain channel matrix¹, and \mathbf{w} denotes the additive white Gaussian noise (AWGN) vector with variance σ^2 . Specifically, \mathbf{H} is defined as

$$\mathbf{H} = \sum_{r=0}^{R-1} h_r \mathbf{\Pi}_{MN}^{l_r} \mathbf{\Delta}_{MN}^{k_r}, \quad (28)$$

¹The delay and Doppler shifts are assumed to be integers.

Fig. 2. SC-IFDM to FMCW, $M = 32, N = 32$.

where l_r , k_r , and h_r denote the delay, Doppler shifts, and channel coefficients of the r -th path, respectively. The matrix $\mathbf{\Pi}_{MN}^{l_r}$ is a permutation matrix with elements $\Pi_{MN}^{l_r}(k, l) = \delta([l - k]_{MN} - l_r)$, and $\mathbf{\Delta}_{MN}^{k_r}$ is an $MN \times MN$ diagonal matrix defined as

$$\mathbf{\Delta}_{MN}^{k_r} = \text{diag} [z_r^0, z_r^1, \dots, z_r^{MN-1}], \quad (29)$$

where $z_r = e^{\frac{j2\pi k_r}{MN}}$. Thus, the transformed received SC-IFDM signal, $\hat{\mathbf{Y}}^{\text{SC-IFDM}}$, can be expressed as

$$\hat{\mathbf{Y}}^{\text{SC-IFDM}} = \underbrace{(\mathbf{I}_N \otimes \mathbf{F}_M^H) \mathbf{\Gamma}^H \mathbf{F}_{MN} \mathbf{H} \mathbf{F}_{MN}^H \mathbf{\Gamma} (\mathbf{I}_N \otimes \mathbf{F}_M)}_{\mathbf{H}_{\text{eff}}^{\text{SC-IFDM}}} \mathbf{X}^{\text{SC-IFDM}} + (\mathbf{I}_N \otimes \mathbf{F}_M^H) \mathbf{\Gamma}^H \mathbf{F}_{MN} \mathbf{w}, \quad (30)$$

while the received and transformed OTFS signal can be written as

$$\hat{\mathbf{Y}}_{\text{SC-IFDM}}^{\text{OTFS}} = \underbrace{\mathbf{\Psi}^H \mathbf{H}_{\text{eff}}^{\text{SC-IFDM}} \mathbf{\Psi}}_{\mathbf{H}_{\text{eff}}^{\text{OTFS}}} \mathbf{x}^{\text{OTFS}} + \mathbf{\Psi}^H (\mathbf{I}_N \otimes \mathbf{F}_M^H) \mathbf{\Gamma}^H \mathbf{F}_{MN} \mathbf{w}. \quad (31)$$

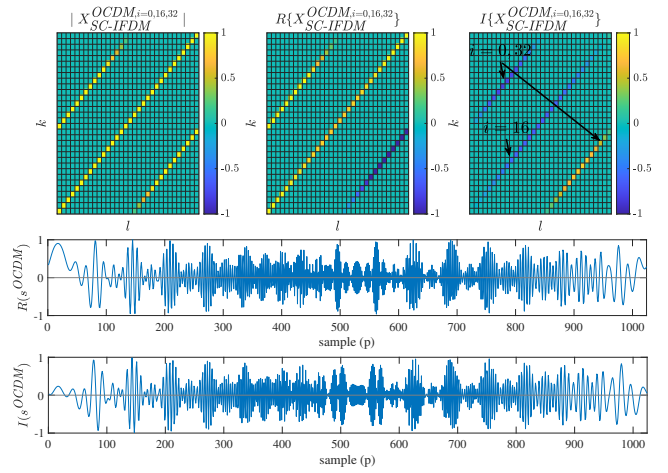
Therefore, OTFS and SC-IFDM can achieve similar performance under doubly dispersive channels, as one can be derived from the other through appropriate phase adjustments. Additionally, an SC-IFDM receiver can extract OTFS data, and vice versa.

C. SC-IFDM to FMCW

Taking $p = l + nM$, the discrete FMCW signal in (16) can be expressed in the SC-IFDM domain using the inverse transform of (7), i.e.,

$$\begin{aligned} X_{\text{SC-IFDM}}^{\text{FMCW}}(k, l) &= \frac{1}{\sqrt{N}} \sum_{n=0}^{N-1} s^{\text{FMCW}}(l + nM) e^{-j2\pi \frac{k(l+nM)}{MN}} \\ &= \frac{e^{j\pi(\frac{l^2}{MN})} \omega_k^l}{\sqrt{N}} \sum_{n=0}^{N-1} e^{j2\pi \frac{(\frac{M}{2}n^2 + (l-k)n)}{N}}. \end{aligned} \quad (32)$$

Note that $e^{j\pi n} = 1$ for even n and -1 for odd n . Similarly, n^2 is even when n is even and odd when n is odd. Given

Fig. 3. SC-IFDM to OCDM, $M = 32, N = 32$.

that $M \in \mathbb{Z}$, it follows that $e^{j\pi(Mn^2)} = (-1)^{Mn^2} = (-1)^{Mn}$. Incorporating this result into (32), we obtain

$$X_{\text{SC-IFDM}}^{\text{FMCW}}(k, l) = \frac{e^{j\pi(\frac{l^2}{MN})} \omega_k^l}{\sqrt{N}} \sum_{n=0}^{N-1} e^{j2\pi \frac{(\frac{M}{2} + l - k)n}{N}}. \quad (33)$$

The elements of the matrix $X_{\text{SC-IFDM}}^{\text{FMCW}}(k, l)$ are nonzero only when $[\frac{M}{2} + l - k]_N = 0$, leading to a sparsity condition where the matrix is nonzero for certain values of l , as depicted in Fig. 2. Specifically, $X_{\text{SC-IFDM}}^{\text{FMCW}}(k, l)$ simplifies to $s^{\text{FMCW}}(l) \omega_k^l$ for the valid solutions corresponding to each $l = 0, \dots, M-1$. This results in a sparse matrix representation, where only M nonzero elements exist in the DFT-based space of the SC-IFDM. Thus, FMCW signaling can be efficiently generated using SC-IFDM by selecting the first M samples from s^{FMCW} based on this sparsity condition. This approach offers a computationally efficient method to integrate the advantages of FMCW and SC-IFDM for JSAC systems.

D. SC-IFDM to OCDM

The i -th orthogonal chirp (OC) of OCDM in (17) can be expressed as

$$s^{\text{OCDM}, i}(l + nM) = e^{j\frac{\pi}{4}} e^{-j\pi \frac{(l+nM-i)^2}{MN}}. \quad (34)$$

Mapping $x^{\text{OCDM}, i}$ into the SC-IFDM domain gives

$$\begin{aligned} X_{\text{SC-IFDM}}^{\text{OCDM}, i}(k, l) &= \frac{1}{\sqrt{N}} \sum_{n=0}^{N-1} s^{\text{OCDM}, i}(l + nM) e^{-j2\pi \frac{k(l+nM)}{MN}} \\ &= \frac{e^{j\frac{\pi}{4}} e^{j\pi \frac{(l-i)^2}{MN}} \omega_k^l}{\sqrt{N}} \sum_{n=0}^{N-1} e^{j2\pi \frac{(-\frac{M}{2}n^2 + (i-l-k)n)}{N}}. \end{aligned} \quad (35)$$

The sparsity of OCDM in SC-IFDM is apparent, as nonzero elements occur only at M specific points, as illustrated in Fig. 3. Consequently, OCDM signals can be efficiently generated within the SC-IFDM framework by leveraging this sparse representation. To demonstrate this, (35) can be rewritten as

$$X_{SC-IFDM}^{OCDM,i}(k,l) = \frac{e^{-j\frac{\pi}{4}} e^{j\pi\left(\frac{l-i}{MN}\right)^2} \omega_k^l}{\sqrt{N}} \sum_{n=0}^{N-1} e^{j2\pi\left(\frac{-M}{2} + i - l - k\right)\frac{n}{N}}. \quad (36)$$

For each i -th element, the condition $\left[\frac{-M}{2} + i - l - k\right]_N = 0$ has a single solution for each $l = 0, \dots, M-1$. For each $[i]_N$, the OCs overlap at the same l, k indices, which demonstrates that OCDM is sparse and represented by only M nonzero points in SC-IFDM space, as shown in Fig. 3. An $M \times N$ OCDM signal consists of M non-overlapping orthogonal signals, such as for $i = 16$ (occupying distinct indices), each containing N overlapping orthogonal signals in SC-IFDM on the same k, l indices, such as for $i = 0$ and $i = 32$ (occupying the same indices while maintaining orthogonality).

E. SC-IFDM to AFDM

Taking $p = l + nM$ in (22), i -th AFDM chirp element can be mapped to the SC-IFDM as

$$\begin{aligned} X_{SC-IFDM}^{AFDM,i}(k,l) &= \frac{1}{\sqrt{N}} \sum_{n=0}^{N-1} s^{AFDM,i}(l+nM) e^{-j2\pi\left(\frac{k(l+nM)}{MN}\right)} \\ &= \frac{s^{AFDM,i}(l) \omega_k^l}{\sqrt{N}} \sum_{n=0}^{N-1} e^{j2\pi\left(\frac{c_1 NM^2 n^2 + (i+c_1 2MNl-k)n}{N}\right)}. \end{aligned} \quad (37)$$

By setting $c_1 = \frac{c'_1}{2MN}$, (37) can be given as

$$X_{SC-IFDM}^{AFDM,i}(k,l) = \frac{s^{AFDM,i}(l) \omega_k^l}{\sqrt{N}} \sum_{n=0}^{N-1} e^{j2\pi\left(\frac{c'_1 \frac{M}{2} + c'_1 l + i - k}{N}\right)n}. \quad (38)$$

Therefore, AFDM is sparse, and $X_{SC-IFDM}^{AFDM,i}(k,l)$ is nonzero only if $\left[c'_1 \frac{M}{2} + c'_1 l + i - k\right]_N = 0$, i.e., for each i -th chirp, there are only M solutions with a more sparse representation where, for each l , there are c'_1 solutions. Thus, AFDM can be represented by only M nonzero points in the SC-IFDM space, as illustrated in Fig. 4. For each $[i]_N$, the AFDM twisted chirps overlap at the same l and k indices. Hence, the AFDM signal can be generated using SC-IFDM. Notably, the element $X_{SC-IFDM}^{AFDM,i}(k,l)$ exhibits a spreading pattern over the $[i]_N$ indices in the twisted TF chirp domain of AFDM. As a result, SC-IFDM is also sparse in the twisted chirp domain, allowing AFDM to be efficiently generated within the SC-IFDM structure.

F. Proposed Mother Waveform

We have shown that OFDM, OTFS, FMCW, OCDM, and AFDM can be efficiently generated using the unified SC-IFDM framework. This insight extends to other advanced waveforms, such as generalized frequency division multiplexing (GFDM), zero-tail OFDM (ZT-OFDM), unique word OFDM (UW-OFDM), Enhanced UW-OFDM, and UW DFT-S-W-OFDM, which share similar structural foundations, as noted in [2]. These structural commonalities inspire the development of a generalized "mother waveform" based on SC-IFDM, from which all other waveforms can be derived through simple phase adjustments and customized data allocation techniques.

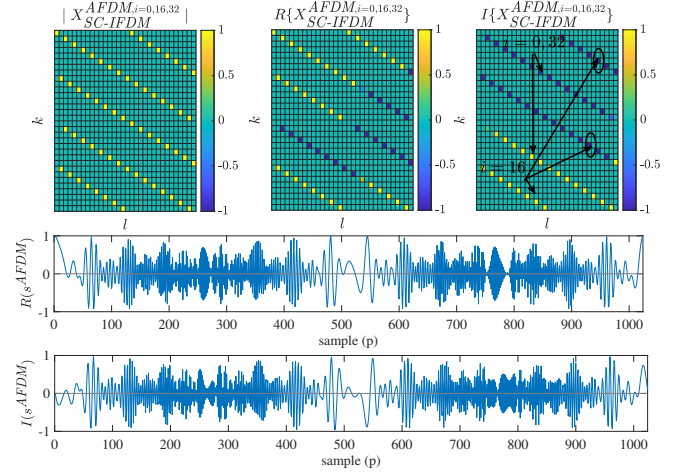


Fig. 4. SC-IFDM to AFDM $M = 32, N = 32, c'_1 = 2, c_2 = 1$.

The primary advantage of this approach lies in its backward compatibility with existing systems, requiring no hardware modifications. This framework capitalizes on current infrastructure, offering a cost-effective pathway to introducing new waveforms without the need for substantial upgrades. By generating all DFT-based waveforms from a single versatile structure, the proposed framework provides a dynamic PHY that can adapt to a wide range of applications, offering flexibility in both waveform design and resource allocation.

As illustrated in Fig. 5, this mother waveform framework systematically generates various waveforms by adjusting how data blocks are allocated, either through interleaving or direct mapping. It allows targeted waveform creation through specific mappings in the grid k and l indices. This flexibility enables seamless orthogonal coexistence of multiple waveforms, allowing 4G, 5G, and 6G systems to support diverse applications with minimal interference. Moreover, this approach enhances the scalability and adaptability of communication systems, enabling the coexistence of multiple waveforms within the same TF resources. It offers a robust solution that meets the evolving demands of future wireless networks, balancing high performance with the seamless integration of heterogeneous services. By facilitating smooth transitions between generations and efficiently managing spectrum resources, the proposed framework ensures that both current and future applications can coexist without requiring changes to the existing hardware infrastructure, making it a highly scalable and future-proof solution for next-generation networks.

IV. PRACTICAL CO-EXISTENCE STRATEGIES OF THE PROPOSED APPROACH FOR 6G

To emphasize the effective integration across the TF domain discussed in the previous section, this work explores orthogonal co-existence capabilities between OTFS or SC-IFDM and OFDM, as well as between SC-IFDM and AFDM. First, we introduce a novel resource allocation strategy for OTFS, designed to facilitate its orthogonal co-existence with other

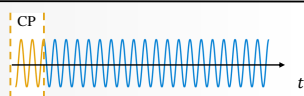
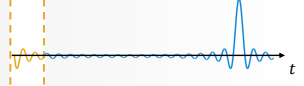
Waveform	Constraint	Spreading	Waveform Generation	Time domain
OFDM	$M = 1$	Time	Data $\rightarrow I_N \rightarrow$ Mapping $\rightarrow F_{MN}^H \rightarrow$ P/S & CP	
DFT-S-OFDM/ SC-FDM	/	Frequency	Data $\rightarrow F_M \rightarrow$ Mapping $\rightarrow F_{MN}^H \rightarrow$ P/S & CP	
SC-IFDM	/	Time-Frequency	Data $\rightarrow F_M \rightarrow$ INT $\rightarrow F_{MN}^H \rightarrow$ P/S & CP	
OTFS	/	Time-Frequency	Data $\rightarrow \omega_l^k \rightarrow F_M \rightarrow$ INT $\rightarrow F_{MN}^H \rightarrow$ P/S & CP	
FMCW/LoRa	$\lfloor \frac{M}{2} + l - k \rfloor_N = 0$	Time-Frequency Diagonal	Data $\rightarrow \omega_l^k \rightarrow F_M \rightarrow$ INT $\rightarrow F_{MN}^H \rightarrow$ P/S & CP	
OCDM	$\lfloor \frac{M}{2} + i - l - k \rfloor_N = 0$	Time-Frequency Diagonal	Data $\rightarrow \omega_l^k \rightarrow F_M \rightarrow$ INT $\rightarrow F_{MN}^H \rightarrow$ P/S & CP	
AFDM	$\lfloor c_1' \frac{M}{2} + i + c_1' l - k \rfloor_N = 0$	Time-Frequency Flexible	Data $\rightarrow \omega_l^k \rightarrow F_M \rightarrow$ INT $\rightarrow F_{MN}^H \rightarrow$ P/S & CP	

Fig. 5. SC-IFDM as a mother waveform to all DFT waveforms and illustration of the resulting signals in time domain.

waveforms. Second, we discuss a specific scenario demonstrating orthogonal co-existence between OTFS and OFDM. Lastly, we propose a method for achieving orthogonal co-existence between SC-IFDM and AFDM. These discussions highlight the effectiveness of the mother waveform concept in supporting orthogonal co-existence while demonstrating its versatility to extend beyond the presented cases for diverse applications.

A. OTFS and SC-IFDM Resource Allocation Scheme

Both OTFS and SC-IFDM distribute data across the entire TF domain to capture delay and Doppler information. However, this inherently prevents orthogonal co-existence with other waveforms within the same resources. Additionally, when an OTFS or SC-IFDM user requires less data than the total grid, the data must still occupy the entire TF resources to maintain delay and Doppler resolution, leading to reduced SE. To address this limitation, we propose a method to optimize resource allocation in the TF domain without compromising the delay and Doppler representation or resolution. This approach leverages the inherent capability of the OTFS system to map TF resources using the ISFFT transform. The delay and Doppler resolution remain dependent solely on the system's bandwidth and symbol duration, ensuring efficient and flexible allocation.

Consider an OTFS system with $\frac{MN}{\alpha\beta}$ data bins, represented as $x[k', l']$, where $k' = 0, \dots, \frac{N}{\alpha} - 1$ and $l' = 0, \dots, \frac{M}{\beta} - 1$. Our approach employs a Kronecker product with a precoding matrix to precisely allocate resources in the TF domain, mathematically expressed as

$$\mathbf{X}_{pr} = \mathbf{P} \otimes \mathbf{X}, \quad (39)$$

where the precoding matrix is defined as

$$\mathbf{P}_{q_1, q_2} = \mathbf{f}_{q_1}^H \mathbf{f}_{q_2}. \quad (40)$$

Here, $\mathbf{f}_{q_1}^H$ denotes the conjugate of the q_1 -th column of the $\alpha \times \alpha$ DFT matrix, and \mathbf{f}_{q_2} represents the q_2 -th row of the $\beta \times \beta$ DFT matrix. The matrix in (40) can be written explicitly as

$$P_{q_1, q_2}[a, b] = \frac{1}{\sqrt{\alpha\beta}} e^{\left\{ \frac{-aq_1}{\alpha} + \frac{bq_2}{\beta} \right\}}, \quad (41)$$

where $e\{\cdot\} = e^{j2\pi(\cdot)}$, $a = \lfloor \frac{k\alpha}{N} \rfloor$, and $b = \lfloor \frac{l\beta}{M} \rfloor$. Therefore, the precoded signal, \mathbf{X}_{pr} , is expressed as

$$X_{pr}[k, l] = \frac{1}{\sqrt{\alpha\beta}} X_s(\lfloor \frac{k\alpha}{N} \rfloor, \lfloor \frac{l\beta}{M} \rfloor) e^{\left\{ \frac{-aq_1}{\alpha} + \frac{bq_2}{\beta} \right\}}. \quad (42)$$

By substituting $k = k' + a\frac{N}{\alpha}$ and $l = l' + b\frac{M}{\beta}$ into (11), where $k' = 0, \dots, \frac{N}{\alpha} - 1$ and $l' = 0, \dots, \frac{M}{\beta} - 1$, the TF domain signal is given by

$$X_{TF}[n, m] = \frac{1}{\sqrt{MN\alpha\beta}} \sum_{a=0}^{\alpha-1} \sum_{b=0}^{\beta-1} \sum_{k'=0}^{\frac{N}{\alpha}-1} \sum_{l'=0}^{\frac{M}{\beta}-1} x_s[k', l'] \times e^{\left\{ \frac{n(k' + \frac{aN}{\alpha})}{N} - \frac{m(l' + \frac{bM}{\beta})}{M} \right\}} e^{\left\{ \frac{bq_2}{\beta} - \frac{aq_1}{\alpha} \right\}}. \quad (43)$$

After simplification, $X_{TF}[n, m]$ can be written as

$$X_{TF}[n, m] = \frac{\psi}{\sqrt{\alpha\beta}} \sum_{a=0}^{\alpha-1} \sum_{b=0}^{\beta-1} e^{\left\{ \frac{a(n - q_1)}{\alpha} - \frac{b(m - q_2)}{\beta} \right\}}, \quad (44)$$

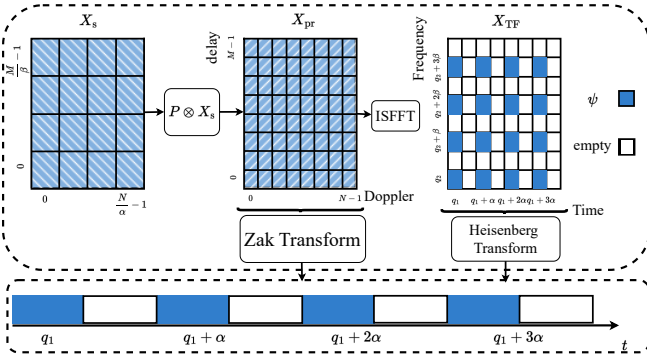


Fig. 6. Proposed OTFS resource allocation ($\alpha = 2, \beta = 2$).

where $\psi = \frac{1}{\sqrt{MN}} \sum_{k'=0}^{N-1} \sum_{l'=0}^{M-1} x_s[k', l'] e^{\left\{ \frac{nk'}{N} - \frac{ml'}{M} \right\}}$. To further simplify $X_{TF}[n, m]$, (44) can be expressed as a product of two Kronecker delta functions as follows

$$X_{TF}[n, m] = \psi \delta_{nq_1} \delta_{mq_2} = \psi \sum_{a=0}^{\alpha-1} e^{\left\{ \frac{a(n-q_1)}{\alpha} \right\}} \sum_{b=0}^{\beta-1} e^{\left\{ \frac{b(q_2-m)}{\beta} \right\}}. \quad (45)$$

For $X_{TF}[n, m]$ to be nonzero, both δ_{nq_1} and δ_{mq_2} must be nonzero, which occurs only when $[n - q_1]_\alpha = 0$ and $[m - q_2]_\beta = 0$. Thus, the TF grid for $X_{TF}[n, m]$ can be controlled as

$$X_{TF}[n, m] = \begin{cases} \psi, & [n - q_1]_\alpha = 0 \text{ and } [m - q_2]_\beta = 0, \\ 0, & \text{Otherwise.} \end{cases} \quad (46)$$

This demonstrates that the OTFS grid in TF domain can be controlled by adjusting the precoding matrix $P_{q_1, q_2}[a, b]$, as illustrated in Fig. 6. The parameters α and β define the spacing between active bins in the time and frequency domains, respectively, while q_1 and q_2 specify the starting indices of the active bins in these domains, enabling flexible and efficient resource allocation without degrading OTFS capabilities of representing delay and Doppler efficiently since the same bandwidth and symbol duration is preserved.

B. SC-IFDM/OTFS and OFDM Co-existence

Building on the earlier discussion of waveform flexibility within the SC-IFDM framework, this section addresses the coexistence of SC-IFDM/OTFS with OFDM in a multi-user scenario. Given that OTFS and SC-IFDM are capable of handling high mobility challenges, they are ideal for mobile users. In contrast, OFDM remains highly effective for static users due to its low-complexity frequency-domain equalization and reduced system latency. Ensuring the seamless integration of these waveforms within the same system is critical for optimizing the overall performance. To achieve this, an orthogonal co-existence scheme is necessary, allowing OFDM to serve static users while SC-IFDM or OTFS addresses the needs of mobile users by operating efficiently in the DD domain. In this context, we focus on OTFS as the representative waveform for mobile users. An orthogonal time co-existence approach, combined with the full cyclic prefix (FCP) method described in [22], is used to address interference between OFDM and

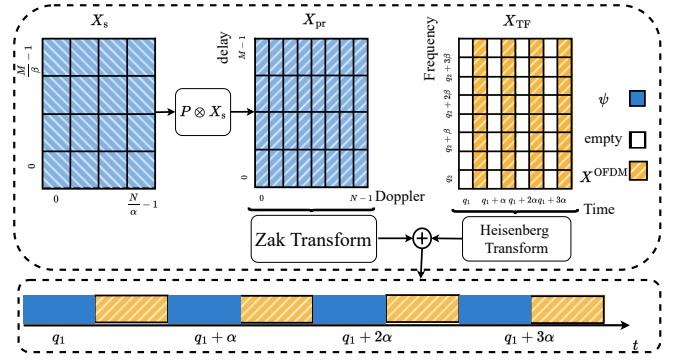


Fig. 7. SC-IFDM/OTFS and OFDM co-existence in time ($\alpha = 2$).

OTFS. In this scheme, OTFS occupies $(\frac{MN}{\alpha})$ data bins after setting $\beta = 1$ and $q_1 = 0$, while OFDM utilizes the remaining $(MN - \frac{MN}{\alpha})$ data bins. This configuration results in (N/α) symbols for OFDM, each with an inverse fast Fourier transform (IFFT) size of M , as illustrated in Fig. 7. The TF grid for this scheme is populated as follows

$$X_{TF}[n, m] = \begin{cases} 0, & [n]_\alpha = 0, \\ X_{OFDM}^{OTFS}(n, m), & \text{Otherwise.} \end{cases} \quad (47)$$

In this approach, OFDM employs IFFT to directly convert data into time, as described in (4), while OTFS is generated through its precoded signal defined in (25) and (42) as follows

$$\mathfrak{s}_{OTFS}(l + nM) = \frac{1}{\sqrt{N}} \sum_{k=0}^{N-1} X_{pr}^{OTFS}(k, l) e^{j2\pi \frac{k(l+nM)}{MN}}, \quad (48)$$

where $X_{pr}^{OTFS}(k, l) = X^{OTFS}(\lfloor k \rfloor \frac{N}{\alpha}, l) e^{j2\pi (\frac{-a}{\alpha})} e^{j2\pi (\frac{-kl}{MN})}$. After transforming X_{TF} to time domain using the Heisenberg transform in (12) and setting $l = m$, the resulting output signal, $\mathfrak{s}_{OFDM}^{OTFS}$, is obtained as

$$\mathfrak{s}_{OFDM}^{OTFS}(l + nM) = \begin{cases} \mathfrak{s}_{OTFS}(l + nM), & [n]_\alpha = 0, \\ \mathfrak{s}_{OFDM}(l + nM), & \text{Otherwise.} \end{cases} \quad (49)$$

The combined signal for both OTFS and OFDM is then formed, ensuring that each waveform operates in its designated TF resources without interference. This method enables efficient co-existence by leveraging the unique strengths of OTFS in handling mobility and doubly selective channels, while OFDM serves static users with low-complexity processing. After the transmission of the combined signal, the received signal undergoes specialized processing to separate and equalize the two channels.

1) OTFS received signal

The received combined signal, y_{OFDM}^{OTFS} , after propagating through the doubly selective channel defined in (28), undergoes initial processing to isolate the OTFS contribution. This involves removing the FCP and applying a weighting vector to isolate OTFS signal. The weighted OTFS signal is then expressed as

$$\hat{y}_{OFDM}^{OTFS}(l + nM) = y_{OFDM}^{OTFS}(l + nM) \cdot G_1(l + nM), \quad (50)$$

where $G_1(l + nM)$ is a binary weighting vector defined as

$$G_1(l + nM) = \begin{cases} 1, & [n]_\alpha = 0, \\ 0, & \text{Otherwise.} \end{cases} \quad (51)$$

This operation effectively filters out the OTFS components, leaving the OTFS signal clean. The DD domain OTFS signal, Y_{DD}^{OTFS} , can be expressed as

$$Y_{DD}^{\text{OTFS}}(k, l) = \sum_{r=0}^{R-1} h_r e^{j2\pi k_r \frac{(L_{FCP} + l - l_r)}{(M + L_{FCP})N}} X_{pr}^{\text{OTFS}}([k - k_r]_N, [l - l_r]_M), \quad (52)$$

where L_{FCP} is the FCP length. The received OTFS signal is thus free of interference from OFDM and can be processed using any known equalization methods. The effective DD channel will exhibit α replicas of channel and any standard equalization technique can be applied to recover the transmitted data.

2) OFDM received signal

For the static channel OFDM user, after passing through a frequency selective channel (where all $k_r = 0$ in (28)), the received signal, $y_{\text{OFDM}}^{\text{SC-IFDM}}$, is similarly processed. By discarding the FCP and applying different weighting vector, the OFDM signal can be expressed as

$$\tilde{y}^{\text{OFDM}}(l + nM) = y_{\text{OFDM}}^{\text{OTFS}}(l + nM) \cdot G_2(l + nM), \quad (53)$$

where $G_2(l + nM)$ is a weighting vector defined as

$$G_2(l + nM) = \begin{cases} 0, & [n]_\alpha = 0, \\ 1, & \text{Otherwise.} \end{cases} \quad (54)$$

This process effectively removes the OTFS components from the signal, isolating the OFDM portion. The resulting frequency-domain OFDM signal, $Y_{\text{Freq}}^{\text{OFDM}}$, can be written as

$$Y_{\text{Freq}}^{\text{OFDM}}(n, m) = \begin{cases} 0, & [n]_\alpha = 0, \\ \sum_{r=0}^{R-1} \bar{h}_r X^{\text{OFDM}}(n, m), & \text{Otherwise,} \end{cases} \quad (55)$$

where $\bar{h}_r = h_r e^{-\frac{j2\pi m r n}{M}}$. This received OFDM signal can then be processed using standard equalization techniques such as minimum mean square error (MMSE) or zero forcing (ZF), ensuring that the signal is free from any OTFS interference and can be equalized effectively.

C. SC-IFDM/OTFS and AFDM Co-existence

In this subsection, we explore the co-existence of SC-IFDM/OTFS and AFDM waveforms within a JSAC system. In such scenarios, OTFS/SC-IFDM is employed for communication in dynamic environments, while orthogonal twisted chirps from AFDM are used for sensing or communication, depending on the AFDM receiver's requirements. The number of twisted chirps can be flexibly allocated based on the needs of both sensing and communication tasks, allowing dynamic resource slicing. Either OTFS or SC-IFDM can be generated based on the waveform selected by the receiver. For demonstration, we

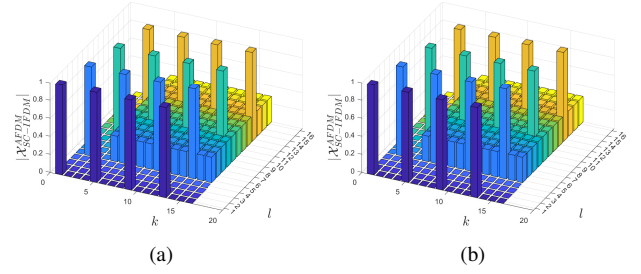


Fig. 8. Proposed SC-IFDM-AFDM in SC-IFDM domain ($c'_1 = 4, M = 16, N = 16$), (a) transmitter side (b) receiver side.

use SC-IFDM to illustrate orthogonal co-existence, expressed as

$$\mathcal{X}_{\text{SC-IFDM}}^{\text{AFDM}}(k, l) = \begin{cases} s^{\text{AFDM}, i}(l) e^{-j2\pi(\frac{kl}{MN})}, & \left[c'_1 \frac{l-M}{2} - c'_1 l + i - k \right]_N = 0, \\ X^{\text{SC-IFDM}}(k, l), & \text{Otherwise.} \end{cases} \quad (56)$$

After transforming $\mathcal{X}_{\text{SC-IFDM}}^{\text{AFDM}}$ to the time domain, a reduced cyclic prefix (RCP) is added to the entire frame to avoid discontinuities in AFDM signal, as described in [22]. The received signal at an SC-IFDM receiver signal, can be given as

$$Y_{\text{SC-IFDM}}^{\text{AFDM}}(k, l) = \sum_{r=0}^{R-1} h_r e^{j2\pi \frac{k_r}{N} \frac{l - l_r}{M}} \Lambda_r(k, l) \times \mathcal{X}_{\text{SC-IFDM}}^{\text{AFDM}}([k - k_r]_N, [l - l_r]_M). \quad (57)$$

The twisted chirps, $s^{\text{AFDM}, i}$, can also be used for communication channel estimation by using appropriate c_1 and leaving a guard in the surrounding of any non-zero point of AFDM as shown in Fig.8(a) and 8(b). In terms of sensing, the received signal is mixed in time with the conjugate of the allocated i -th twisted chirp, $\text{conj}(s^{\text{AFDM}, i})$, to estimate the time delay and Doppler shifts introduced by the targets.

It is important to note that AFDM, in addition to its use for sensing, can also be employed for communication within this co-existence framework. The dual use of AFDM for both sensing and communication allows for efficient resource allocation and performance optimization in dynamic JSAC environments.

V. SIMULATION RESULTS

In this section, we evaluate the proposed co-existence schemes in terms of communication and sensing for the proposed systems. The key performance indicators (KPIs) used for communication performance are BER and SE, while for sensing, the KPIs are root mean squared error (RMSE) of the range and velocity. Unless stated otherwise, the key system simulation parameters are summarized in Table I.

A. Communication Co-existence Performance

First, the BER performance of the proposed schemes, including OTFS-OFDM, SC-IFDM-OCDFM, SC-IFDM-AFDM, and SC-IFDM-OTFS, is evaluated. The results are illustrated

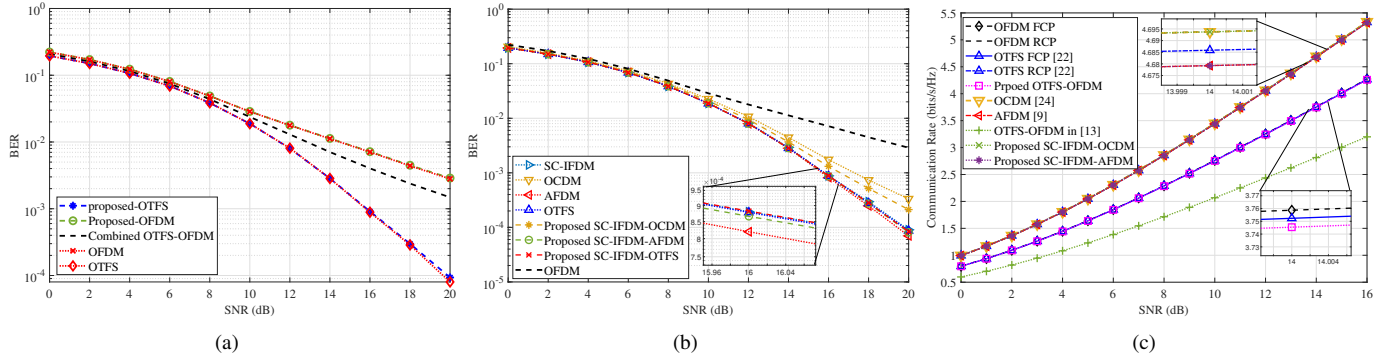


Fig. 9. (a) BER of OTFS/SC-IFDM and OFDM co-existence, (b) BER of the proposed co-existence of SC-IFDM with different waveforms, (c) communication rate vs. SNR analysis.

TABLE I
SIMULATION PARAMETERS

Description	Parameters	Value
Carrier frequency	f_c	77 GHz
Bandwidth	B	200 MHz
Subcarrier spacing	Δf	B/M MHz
No. of sub-carriers per symbol	M	32
No. of OFDM symbols	N	32
No. of SC-IFDM/OTFS symbols	$N_{SC-IFDM}$	200
No. of chirps/SC-IFDM symbol	N_c	1
SC-IFDM-AFDM parameter	$c_1 = 2$	1
Range resolution	Δr	0.7495 m
Velocity resolution	Δv	1.9011 m/s
Range of targets	r_r	$\sim U(0, 100)$ m
Velocity of targets	v_r	$\sim U(-80, 80)$ m/s
Signal-to-noise ratio	SNR	15 dB

in Fig. 9(a) and Fig. 9(b). The proposed OTFS-OFDM scheme demonstrates a BER performance comparable to both the OTFS system discussed in [22] and conventional OFDM. This is illustrated in Fig. 9(a), which depicts both the overall and individual BER performance. A notable feature of this scheme is its integration of OFDM within the OTFS symbol. This integration enhances the SE and reduces latency, allowing OFDM users to decode their data without waiting for the entire OTFS frame to be processed, particularly when the OTFS user requires only (MN/α) data.

Fig. 9(b) illustrates the BER performance of the SC-IFDM-OCDM, SC-IFDM-AFDM, and SC-IFDM-OTFS schemes. SC-IFDM-OCDM demonstrates slightly better BER performance compared to conventional OCDM, reflecting the inherent advantages of SC-IFDM. Meanwhile, SC-IFDM-AFDM and SC-IFDM-OTFS show BER performance comparable to conventional AFDM and OTFS, respectively.

Next, the (SE) of the proposed co-existence waveforms is analyzed. The SE depends on parameters such as frame length, cyclic prefix (CP) size, pilot overhead, and guard intervals. Fig. 9(c) illustrates the SE of the proposed schemes. The results in Fig. 9(c) show that the proposed OTFS-OFDM scheme achieves higher SE than conventional TDD or FDD schemes, as well as the approach proposed in [13], particularly when the OTFS user requires MN/α data. This improvement is

attributed to the integration of OFDM within the OTFS symbol, which enables efficient utilization of the TF resources without sacrificing delay and Doppler resolution.

The SE for the OTFS-OFDM scheme is derived considering MN/α data, with the FCP ensuring a clean signal. The communication rate for OTFS-OFDM is expressed as

$$\mathcal{C}_{OFDM}^{OTFS} = \left(\frac{MN/\alpha - \varphi_{OTFS}}{MN + N L_{FCP}} \log_2(1 + \gamma) \right) + \left(\frac{T/\alpha - \varphi_{OFDM}}{T + T_{cp}} \log_2(1 + \gamma) \right), \quad (58)$$

where γ , φ_{OTFS} , φ_{OFDM} , and α denote the communication signal-to-noise ratio (SNR), pilot and guard overhead of OTFS, pilot and guard overhead of OFDM, and the co-existence ratio, respectively.

Using the SE formulas from [22] and [23], the SE for conventional and other proposed waveforms is calculated as follows

$$\mathcal{C}_{OFDM} = \left(\frac{T - \vartheta_{OFDM}}{T + T_{cp}} \log_2(1 + \gamma) \right), \quad (59)$$

$$\mathcal{C}_{OTFS_{FCP}} = \left(\frac{M - \vartheta_{OTFS}}{M + L_{FCP}} \log_2(1 + \gamma) \right), \quad (60)$$

$$\mathcal{C}_{OCDM} = \left(\frac{MN - \vartheta_{OCDM}}{MN} \log_2(1 + \gamma) \right), \quad (61)$$

$$\mathcal{C}_{AFDM} = \left(\frac{MN - \vartheta_{AFDM}}{MN} \log_2(1 + \gamma) \right), \quad (62)$$

where ϑ_{OCDM} and ϑ_{AFDM} represent the pilot and guard overheads specific to OCDM and AFDM [23], respectively. Finally, the SE of the proposed SC-IFDM-OCDM, SC-IFDM-AFDM, and SC-IFDM-OTFS schemes is analyzed. The SE of these waveforms depends on the number of data symbols and pilots. Due to the orthogonality between these waveforms in the proposed co-existence schemes, their SE can be directly calculated. As illustrated in Fig. 9(c), the proposed SC-IFDM-OCDM, SC-IFDM-AFDM, and SC-IFDM-OTFS waveforms demonstrate no loss in SE compared to their individual use. This result highlights the effectiveness of the proposed mother waveform in maintaining the SE of the constituent waveforms while enabling their coexistence within the same TF resources.

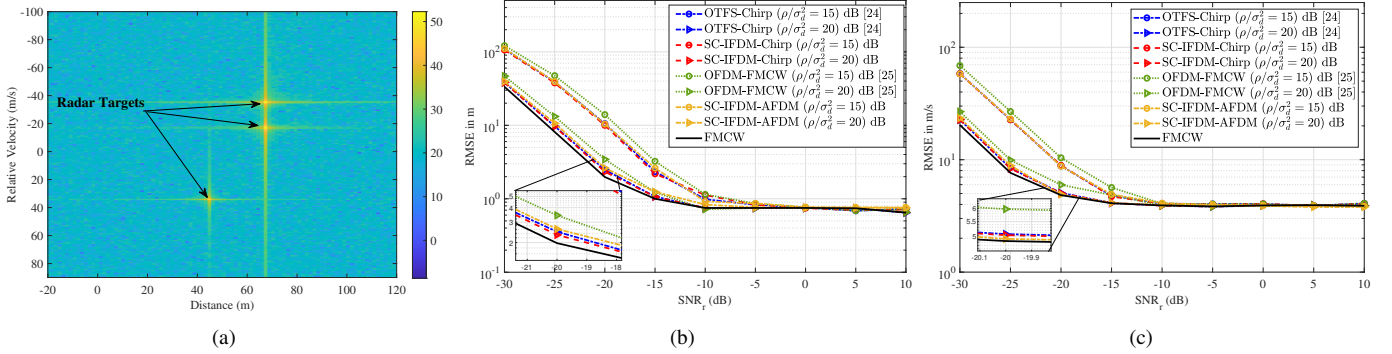


Fig. 10. (a) Range-Doppler map (3 targets), (b) range RMSE performance vs SNR (3 targets), (c) velocity RMSE performance vs SNR (3 targets).

B. Sensing Co-Existence Performance

The sensing performance of the proposed waveforms is evaluated using a range and velocity estimation scenario involving three targets. The results are presented in Fig. 10, which includes: (a) the range-Doppler map, (b) the range RMSE performance versus SNR, and (c) the velocity RMSE performance versus SNR. To quantify sensing accuracy, the RMSE of the range and velocity is analyzed for the proposed SC-IFDM-Chirp and SC-IFDM-AFDM waveforms. For comparison, the performance of existing methods, including OTFS-Chirp [24], OFDM-FMCW [25], and FMCW alone, is also evaluated. For OFDM, which employs multiple orthogonal chirps, the performance of a single chirp is presented to simplify the comparison.

The results, as shown in Fig. 10(b) and Fig. 10(c), demonstrate that the proposed SC-IFDM-Chirp and SC-IFDM-AFDM waveforms achieve performance comparable to OTFS-FMCW. This is due to the inherent similarity between SC-IFDM and OTFS in their ability to represent chirps sparsely, as previously discussed. Furthermore, the proposed schemes exhibit performance close to FMCW with appropriate power allocation. The sensing performance of SC-IFDM-Chirp and SC-IFDM-AFDM depends on the power ratio assigned to the chirp signal ρ/σ_d^2 , where σ_d^2 is the data power. Simulations conducted with two power ratios (15 dB and 20 dB) show that increasing the chirp power ratio significantly improves performance, bringing it closer to that of standalone FMCW. This enhancement results from the higher radar SNR (SNR_r) of the chirp, which directly improves the accuracy of range and velocity estimation.

In contrast, the existing OFDM-FMCW method exhibits inferior performance. This degradation is primarily due to the loss of orthogonality between the chirp signal and data, as well as among the data symbols themselves. The issue arises because the chirp is extracted from the diagonal elements of the DFT matrix, leading to interference. This interference limits sensing accuracy and highlights the importance of designing better waveforms for such systems.

The results demonstrate that the proposed SC-IFDM-Chirp, SC-IFDM-OCDFM, and SC-IFDM-AFDM waveforms provide robust sensing performance comparable to OTFS-FMCW and FMCW, while addressing the limitations of existing methods

such as OFDM-FMCW. The flexibility in power allocation and orthogonality preservation highlights their effectiveness for joint communication and sensing applications.

VI. CONCLUSION

In this paper, we proposed a unified "mother waveform" framework, capable of generating multiple DFT-based waveforms like OTFS, OFDM, FMCW, OCDFM, and AFDM from a single SC-IFDM structure. We showed that these waveforms differ primarily in phase shifts and data allocation strategies, enabling efficient orthogonal coexistence within shared time-frequency resources. This solution supports diverse 4G, 5G, and 6G applications such as URLLC, mMTC, and high-mobility scenarios, while ensuring backward compatibility with existing infrastructure. Our simulations confirmed the framework's effectiveness in achieving low BER, efficient resource allocation, and robust multi-user performance. Future work may focus on real-time implementation on SDR platforms and using artificial intelligence (AI) / machine learning (ML) for dynamic waveform switching, advancing the adaptability and scalability of communication systems for 6G networks and beyond.

REFERENCES

- [1] M. Giordani, M. Polese, M. Mezzavilla, S. Rangan, and M. Zorzi, "Toward 6G networks: Use cases and technologies," *IEEE Commun. Mag.*, vol. 58, no. 3, pp. 55–61, 2020.
- [2] A. Sahin, R. Yang, E. Bala, M. C. Beluri, and R. L. Olesen, "Flexible DFT-S-OFDM: solutions and challenges," *IEEE Commun. Mag.*, vol. 54, no. 11, pp. 106–112, 2016.
- [3] I. RECOMMENDATION, "Framework and overall objectives of the future development of imt for 2030 and beyond," *tech. rep., International Telecommunication Union (ITU) Recommendation (ITU-R), Tech. Rep.*, 2023.
- [4] T. Hwang, C. Yang, G. Wu, S. Li, and G. Y. Li, "OFDM and its wireless applications: A survey," *IEEE Trans. Veh. Technol.*, vol. 58, no. 4, pp. 1673–1694, 2008.
- [5] M. Noor-A-Rahim *et al.*, "6G for vehicle-to-everything (V2X) communications: Enabling technologies, challenges, and opportunities," *Proc. IEEE*, vol. 110, no. 6, pp. 712–734, 2022.
- [6] G. Berardinelli, F. M. L. Tavares, T. B. Sørensen, P. Mogensen, and K. Pajukoski, "Zero-tail DFT-spread-OFDM signals," in *Proc. Globecom Workshops*, Dec. 2013, pp. 229–234.
- [7] A. Sahin, R. Yang, M. Ghosh, and R. L. Olesen, "An improved unique word DFT-spread OFDM scheme for 5G systems," in *2015 IEEE Globecom Workshops (GC Wkshps)*, San Diego, CA, USA, 2015, pp. 1–6.

- [8] R. Hadani, S. Rakib, M. Tsatsanis, A. Monk, A. J. Goldsmith, A. F. Molisch, and R. Calderbank, "Orthogonal time frequency space modulation," in *Proc. IEEE Wireless Commun. Netw. Conf. (WCNC)*, Mar. 2017, pp. 1–6.
- [9] A. Bemani, N. Ksairi, and M. Kountouris, "AFDM: A full diversity next generation waveform for high mobility communications," in *Proc. IEEE Int. Conf. Commun. Workshops (ICC Workshops)*, Jun. 2021, pp. 1–6.
- [10] M. S. Omar and X. Ma, "Performance analysis of OCDM for wireless communications," *IEEE Trans. Wireless Commun.*, vol. 20, no. 7, pp. 4032–4043, 2021.
- [11] S. Li, J. Yuan, W. Yuan, Z. Wei, B. Bai, and D. W. K. Ng, "Performance analysis of coded ofts systems over high-mobility channels," *IEEE Trans. Wireless Commun.*, vol. 20, no. 9, pp. 6033–6048, 2021.
- [12] A. Bemani, N. Ksairi, and M. Kountouris, "Affine frequency division multiplexing for next generation wireless communications," *IEEE Trans. Wireless Commun.*, vol. 22, no. 11, pp. 8214–8229, 2023.
- [13] M. S. J. Solaija, S. E. Zegrar, and H. Arslan, "Orthogonal frequency division multiplexing: The way forward for 6G physical layer design?" *IEEE Veh. Technol. Mag.*, vol. 19, no. 1, pp. 45–54, 2024.
- [14] V. Winkler, "Range doppler detection for automotive FMCW radars," in *Proc. Eur. Radar Conf.*, Munich, Germany, October 2007, pp. 166–169.
- [15] M. Alizadeh *et al.*, "Remote monitoring of human vital signs using mm-wave FMCW radar," *IEEE Access*, vol. 7, pp. 54 958–54 968, 2019.
- [16] H. G. Myung, J. Lim, and D. J. Goodman, "Single carrier FDMA for uplink wireless transmission," *IEEE Veh. Technol. Mag.*, vol. 1, no. 3, pp. 30–38, 2006.
- [17] N. Benvenuto, R. Dinis, D. Falconer, and S. Tomasin, "Single carrier modulation with nonlinear frequency domain equalization: An idea whose time has come—again," *Proc. IEEE*, vol. 98, no. 1, pp. 69–96, 2010.
- [18] F. Lampel, A. Avarado, and F. M. Willems, "On OTFS using the discrete Zak transform," in *Proc. IEEE Int. Conf. Commun. Workshops (ICC Workshops)*, Seoul, Korea, Republic of, May 2022, pp. 729–734.
- [19] M. W. Chia, B. S. Thian, and T. T. Tjhung, "Distributed DFT-spread OFDM," in *Proc. IEEE Singapore Int. Conf. Commun. Syst.*, Oct./Nov. 2006, pp. 1–5.
- [20] M. Mert Şahin and H. Arslan, "Multi-functional coexistence of radar-sensing and communication waveforms," in *Proc. IEEE 92nd Veh. Technol. Conf. (VTC-Fall)*, 2020, pp. 1–5.
- [21] X. Ouyang and J. Zhao, "Orthogonal chirp division multiplexing," *IEEE Trans. Commun.*, vol. 64, no. 9, pp. 3946–3957, 2016.
- [22] S. E. Zegrar and H. Arslan, "Effect of prefix/suffix configurations on ofts systems with rectangular waveforms," *arXiv preprint arXiv:2205.14872*, 2022.
- [23] H. Haif, S. E. Zegrar, and H. Arslan, "Novel ocdm transceiver design for doubly-dispersive channels," *IEEE Trans. Veh. Technol.*, vol. 73, no. 8, pp. 11 237–11 248, 2024.
- [24] S. E. Zegrar, A. A. Boudjelal, and H. Arslan, "A novel OTFS-Chirp waveform for low-complexity multi-user joint sensing and communication," *IEEE Internet Things J.*, pp. 1–1, 2024.
- [25] A. Bouziane, S. E. Zegrar, and H. Arslan, "A novel OFDM-FMCW waveform for low-complexity joint sensing and communication," *IEEE Wireless Commun. Lett.*, pp. 1–1, 2024.